Malaysian Journal of Chemistry, 2023, Vol. 25(4), 232-245

Hybridization and Characterization of a Deep Eutectic Solvent Molecularly Imprinted Polymer Membrane for the Removal of Bisphenol A

Syed Asim Hussain Shah[1]*, Sity Aishah Mansur[2], Mustafa Humam Sami[3], Rizwana Asghar[4] and Saliza Asman[1]*

[1]Department of Physics and Chemistry, Faculty of Applied Sciences and Technology, University Tun Hussein Onn Malaysia (UTHM), UTHM Pagoh Campus, Pagoh Higher Education Hub, KM 1, Jalan Panchor, 84600 Muar, Johor, Malaysia

[2]Department of Chemical Engineering Technology, Faculty of Engineering Technology, University Tun Hussein Onn Malaysia (UTHM), UTHM Pagoh Campus, Pagoh Higher Education Hub, KM 1, Jalan Panchor, 84600 Muar, Johor, Malaysia

[3]Department of Pharmacy, Al-Noor University College, Nineveh, Iraq

[4]Department of Chemistry and Chemical Engineering, Institute of Molecular Science, Shanxi University Taiyuan 030006, China

*Corresponding author (e-mail: asimshah8896@gmail.com; salizaa@uthm.edu.my)

A deep eutectic solvent molecularly imprinted polymer (DES-MIP) was synthesized via bulk polymerization using bisphenol A (BPA) as the template, DES as the monomer, ethylene glycol dimethyl acrylate (EGDMA) as the cross-linker, and benzoyl peroxide (BPO) as the initiator. A hybridized deep eutectic solvent molecular-imprinted polymer membrane (HDES-MIP) was produced by hybridizing cellulose acetate (CA) with a previously prepared DES-MIP. Fourier transform infrared spectroscopy (FTIR) and scanning electron microscopy (SEM) were used to analyze the fundamental functional groups and morphology of the synthesized membrane. Kinetic and isotherm analyses of the HDES-MIP membrane revealed that the data corresponded well with pseudo-second-order kinetic (R^2 = 0.9986) and Langmuir isotherm models (R^2 = 0.9983). The maximum adsorption capacity was observed at pH 8. A thermodynamic study of the HDES-MIP membrane showed that the adsorption of BPA was exothermic and spontaneous. The development of a hybridized deep eutectic solvent molecular-imprinted polymer membrane (HDES-MIP) offers significant potential for the effective and environment-friendly removal of bisphenol A (BPA), emphasizing the importance of this research in addressing pollution concerns and advancing sustainable materials.

Keywords: Hybrid; cellulose acetate; molecularly imprinted membrane; Bisphenol A; deep eutectic solvent

Received: June 2023; Accepted: August 2023

Bisphenol A (BPA) is an emerging organic, synthetic, and chemical intermediate used to produce certain plastics and epoxy resins [1]. BPA is one of the most widespread endocrine disruptors that causes chronic health conditions related to the reproductive system, metabolic function, nervous system, immune function, and growth [2]. BPA has been banned in the production of baby bottles with other food contact items for children under the age of three. The European Chemical Agency (ECHA) has classified BPA as a chemical of high concern. Recent rules have placed even more restrictions on the use of BPA, which is why food manufacturers are steadily looking for alternatives to eliminate BPA from their products [3]. The European Commission approved a regulation in 2018 that restricts the use of BPA as a packing material. The Specific Migration Limit (SML) per kilogram of food was reduced from 0.6 mg to 0.05 mg. For body weight, 4 µg/kg was set as the new Tolerable Daily Intake (t-TDI) [4]. The US Environmental Protection Agency declared BPA a substance of very high concern [5]. Several techniques including chemical oxidation [1], catalytic oxidation [6], and microbial degradation [7] have been used to extract BPA. However, these techniques are expensive and can produce secondary pollutants. Therefore, it is crucial to consistently search for affordable and reliable adsorption methods.

Molecularly imprinted polymers (MIPs) are synthetic materials with specially designed binding sites and are used in various industries [8]. MIPs are being used as a separation material for different compounds, such as pesticides [9], drugs [10], and amino acids [11]. MIP synthesis requires less time and is comparatively less expensive than many other purification techniques, such as coagulation [12], biological treatment [13], catalytic oxidations [6], ozonation solvent extraction [14], and adsorption

distillation [15]. Owing to these advantages, conventional MIPs still face the problems of low binding capacity and low selectivity [16]. Deep eutectic solvents (DESs) are emerging solvents that have been gradually applied as functional monomers for molecular imprinting [17]. DESs are composed of a hydrogen bond acceptor (HBA) and a hydrogen bond donor (HBD), and the resultant compounds have lower melting points than the individual constituents [18]. The components are bonded via van der Waals forces and hydrogen bonding. DESs possess excellent characteristics, including cheaper price, higher functional capacity, and low toxicity [19].

In recent years, MIP-based membranes have attracted considerable interest. Numerous articles on the fabrication of MIP membranes have been published, demonstrating distinct permeabilities and separations for ligands/templates, such as nucleotides [20], cholesterol [21], and many other drugs [22]. Cellulose acetate is ideal for fabricating MIP membranes owing to its porosity, chemical stability, and bio-compatibility. MIP membranes can be easily processed into thin films, possess functional groups for modification, and allow for high selectivity in target-molecule binding [23]. MIPs conjugated to quantum dots (QDs) were successfully used to create an imprinted cellulose membrane for specific myoglobin (Myo) recognition [24]. The resulting membrane displayed high sensitivity, stability, and selectivity, making it a promising portable and user-friendly system for point-of-care Myo detection. In addition, research has been conducted on the transport characteristics and sensor technology applications of MIP membranes [25].

To the best of our knowledge, the use of deep eutectic solvents (DESs) in the synthesis of molecularly imprinted polymers (MIPs) and their application in membranes have not been previously reported. In this study, we developed a novel approach employing choline chloride-methacrylic acid (ChCl-MAA) as a functional monomer in the bulk polymerization process to create a highly precise and effective DES-MIP. The synthesized DES-MIP was then incorporated into a cellulose acetate membrane (HDES-MIP) to remove bisphenol A (BPA) from aqueous solutions. The HDES-MIP membrane was comprehensively characterized using Fourier transform infrared spectroscopy (FTIR) and scanning electron microscopy (SEM) to analyze its functional groups and morphology, respectively. This study presents a pioneering approach for the synthesis of MIPs using DESs, and demonstrates their successful application as efficient sorbents for the removal of BPA from aqueous solutions. Detailed characterization and thorough exploration of the optimization parameters contribute to a comprehensive understanding of the capabilities and potential of HDES-MIP membranes in various environmental and industrial applications.

EXPERIMENTAL

1. Chemicals

All reagents used in this study were of analytical grade. Ethylene glycol dimethyl acrylate (EGDMA, 97.5%), methacrylic acid (MAA, 99%), benzoyl peroxide (BPO, 98.0%), bisphenol A (BPA, 99%.0%), acetic acid (CH_3COOH, 98.0%), hydrochloric acid (HCl, 37.0%), sodium hydroxide (NaOH, 98.0%), choline chloride (ChCl, 98.0%), methanol (CH_3OH, 99.8%), cellulose acetate (CA), and acetone (CH_3COCH_3, 99.5%) were purchased from Sigma Aldrich (MERCK).

2. Instruments

Fourier transform infrared spectroscopy was used to identify the key functional groups of CA and HDES-MIP between 4000-400 cm^{-1} (PerkinElmer FTIR Spectrum 100). The morphology was studied using scanning electron microscopy (SEM, JOEL JSM 7600F, USA).

3. Preparation of DES-MIP Particles

DES-MIP was created by mixing 0.032 g of BPA, as a template, with 10 ml of acetonitrile, which contained 0.757 ml of DES, as a monomer; 0.894 ml of EGDMA, as a crosslinker; and an initiator (0.15 g). The mixture was sealed and polymerized for 24 h in a water bath at 70°C, after purging with nitrogen for 5 min. Crushed and pulverized polymers were obtained. Next, a 1:2 (v/v) methanol-acetic acid solution was used to thoroughly wash the template out of the polymer [26].

4. Hybridization of DES-MIP with CA

Phase inversion was used to hybridize DES-MIP particles with cellulose acetate (CA) to synthesize the HDES-MIP membrane. 1.00 g of CA was dissolved in 30.00 mL of acetone. 0.05 g of DES-MIP was added to the CA solution and the mixture was continuously agitated at 50°C to obtain a homogenous mixture. Following the protocol by Yusof et al. (2013), with modifications, the resulting mixture was spread on a glass plate and allowed to dry overnight at room temperature [27]. Figure 1 shows a schematic of the preparation of the HDES-MIP membrane.

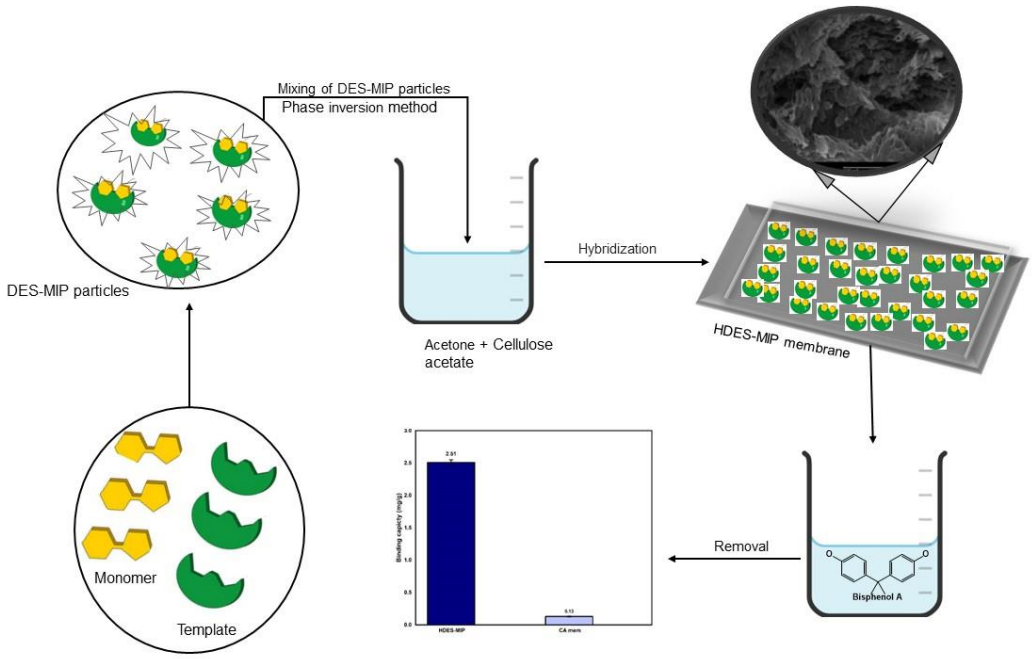

Figure 1. Schematic diagram for preparation of HDES-MIP membrane.

5. Binding Capacity of BPA by HDES-MIP Membrane

It is important to compare the adsorption capacities of the HDES-MIP and CA membranes. 10 mg/L BPA solutions with 0.012 g of HDES-MIP and CA membranes, respectively, were incubated for 1 h. The membranes were then carefully removed from the solutions. The binding capacities of the HDES-MIP and CA membranes were measured using solution–vis spectrometer. The binding capacity was calculated using Eq. (1):

$$Q = \frac{(C_0 - C_f) \times v}{w} \quad (1)$$

Where Q (mg/g) is the amount of BPA adsorbed by HDES-MIP and CA membranes respectively. C_0 (mg/L) and C_f (mg/L) are the initial and equilibrium concentrations of BPA solution, respectively, w (g) is the added amount of HDES-MIP, and v (L) is the volume of the initial BPA solution and CA membranes.

6. Adsorption Studies

Adsorption studies were performed in batch experiments to determine the maximum adsorption capacity of the HDES-MIP membrane**.** Kinetic, isothermal, and pH tests were conducted for this purpose.

6.1. Study of pH Effect

HDES-MIP and CA membranes were shaken for an hour in 10 mL of 10 ppm BPA solutions of different pH from 1 to 12. Basic and acidic pH values were adjusted using NaOH and hydrochloric acid, respectively. The HDES-MIP and CA membranes were incubated in the BPA solutions for 1 h at room temperature. The optimal pH for maximal sorption was determined after the analysis of the BPA solution filtrate.

6.2. Kinetic Study

To 10 mg/L BPA solutions, 0.012 g of HDES-MIP and CA membranes were added, respectively, and the mixtures were mixed for various incubation durations (5, 10, 15, 20, 25, 30, 40, and 50 min). The final BPA concentration was determined to evaluate the optimal period for BPA removal using HDES-MIP and CA membranes. The following equation was used to calculate the adsorption capacity of HDES-MIP and CA over time (t):

$$Q_t = \frac{[(C_0 - C_t) \times v]}{w} \quad (2)$$

Here, CA and HDES-MIP adsorption capacities are denoted by Q_t (mg/g). The final and initial concentrations of the BPA solution are represented as C_t and C_0, respectively (mg/L). The mass of HDES-MIP and CA and the volume of the solution are denoted by w (g) and v (L), respectively.

6.3. Adsorption Kinetic Models

Pseudo second and first order models were applied to analyze the kinetics of BPA adsorption onto CA and HDES-MIP. Correlation coefficient (R^2) was used to express the agreement between experimental and predicted values. When comparing the values, a higher number near or equal to one is used to denote the

kinetic model that best fits the data [28]. Based on the pseudo-first-order model, the rate of change in solute intake over time is proportional to the difference between the saturation concentration and the amount of solid absorbed over time. The following equation can be used to explain the pseudo-first-order model [29].

$$\log(q_e - q_t) = \log q_e - \frac{k_1 t}{2.303} \quad (3)$$

Equation 4 represents the pseudo-second-order.

$$\frac{t}{q_t} = \frac{1}{k_2 q_{e^2}} + \frac{t}{q_e} \quad (4)$$

6.4. Adsorption Isotherm Study

To determine the equilibrium adsorption isotherm at the optimum time, various starting BPA concentrations (5, 10, 15, 20, 25, 30, 35, 40, and 50 mg/L) were investigated at 298 K. Mechanical shaking was used to mix 0.012 g of HDES-MIP and CA, respectively, with varied BPA solution concentrations. Each experiment was performed a maximum of three times, and the average of the three results was used to analyze the outcome. The following equation can be used to compute the binding capacity of BPA at equilibrium, which is represented by the symbol Q_e (mg/g) [30].

$$Q_e = \frac{[(C_0 - C_e) \times v]}{w} \quad (5)$$

The binding capacities of CA and HDES-MIP are represented by Q_e (mg/g). The equilibrium and initial concentrations of the BPA solution are represented by C_e (mg/L) and C_0 (mg/L), respectively. v (L) represents the volume of BPA solution and the mass of MIP particles and DES-MIP is shown by w (g) [31].

6.5. Adsorption Isotherm Models

The ability of the linearized two-parameter equations of Langmuir and Freundlich to reflect equilibrium sorption data was investigated [32]. These parameters provided useful information regarding the affinity, surface characteristics, and sorption mechanisms of the adsorbent. The Langmuir isotherm model was designed based on the idea that the adsorbent has a homogenous structure, with all sorption sites being comparable and energetically equivalent. The general equation for the Langmuir isotherm model is as follows:

$$\frac{C_e}{q_e} = \frac{1}{bq_m} + \frac{C_e}{q_m} \quad (6)$$

Reversible adsorption is explained using the Freundlich isotherm model, which is not only confined to monolayer formation but also the process of sorption on heterogeneous surfaces from aqueous solutions. The general equation for the Freundlich isotherm model is as follows:

$$\log q_e = \log k_f + \frac{1}{n_f} \log C_e \quad (7)$$

6.6. Thermodynamic Study

Adsorption thermodynamics is important for determining the behavior of HDES-MIP and CA with respect to temperature. Three measurements of HDES-MIP and 0.012 g of CA were performed at 298, 318, and 338 K. Following the removal of HDES-MIP and CA from the solutions, the eluates were examined using a UV-visible spectrophotometer to determine the adsorption capacity. To evaluate the spontaneity of the reaction, the thermodynamic characteristics are crucial. To apply the adsorption process, changes in enthalpy ($H°$), Gibbs free energy ($G°$), and entropy ($S°$) were regarded as actual pointers. The degree of spontaneity of the reaction ($G°$) is given by Equation (8):

$$\Delta G^o = \Delta H^o - T\Delta S^o \quad (8)$$

Equation (9) was used to determine the change in entropy ($S°$) and enthalpy ($H°$).

$$ln\, K = \frac{-\Delta H^0}{RT} + \frac{-\Delta S^0}{R} \quad (9)$$

Where R is the ideal gas constant (8.314 J/mol/K) and K (g/L) is the equilibrium constant or distribution coefficient. The temperature in Kelvin is T [33]. $\Delta S°$ and $\Delta H°$ can be recognized from the Van't Hoff plot (ln K vs. 1/T) by calculating the intercept's slope.

RESULTS AND DISCUSSION

Characterization of DES-MIP and Membranes

The prepared HDES-MIP was characterized using scanning electron microscopy (SEM) and Fourier transform infrared (FTIR) spectroscopy for comparison with DES-MIP particles and CA membranes.

1. Analysis of Functional Groups

Figure 2 shows the FTIR spectra of HDES-MIP, CA, and DES-MIP powders. C-O-C and C=O stretchings were detected in the spectrum of the CA membrane at 1735 cm^{-1} and 1032 cm^{-1}, respectively. The C-O-C and C=O stretching vibrations were altered to shorter wavenumbers in the spectrum of the HDES-MIP membrane. The C=O and -C-O-C- stretching bands

changed from 1735 cm-1 to 1732 cm^{-1} and 1032 cm^{-1} to 1035 cm^{-1}, respectively. Furthermore, the -OH stretching band at 3371 cm^{-1} and the $-CH_3$ stretching band at 2956 cm^{-1} vanished in the HDES-MIP membrane. These changes in the FTIR spectra revealed that the DES-MIP and CA membranes interacted. The spectra shifted from those of the CA membrane to those of the HDES-MIP membrane. The successful hybridization of the DES-MIP particles with the CA polymer-producing HDES-MIP membrane was demonstrated by the shifts in the spectra from the CA membrane to the HDES-MIP membrane.

2. Morphological Analysis

The morphologies of the HDES-MIP and CA membranes are shown in Figure 3. The morphologies of the HDES-MIP and CA membranes were quite different. The CA membrane exhibited a consistently smooth structure owing to the absence of cavities. This observation is attributed to the absence of DES-MIP particles, and the smooth structure of the CA membrane was changed by the addition of the DES-MIP particles formed by HDES-MIP, resulting in a rougher surface with cavities. This demonstrates the dependability and effectiveness of the hybridization of DES-MIP particles with the CA membrane in solution. The morphology of the HDES-MIP membrane suggests that the DES-MIP particles hybridized well with the CA membrane. A similar study was conducted by Yusof et al., 2013 [27].

Table 1. Functional groups of CA, DES-MIP and HDES-MIP with respect to wavelength.

Material	C-O-C Stretching (cm^{-1})	C=O Stretching (cm^{-1})	-OH Stretching (cm^{-1})	$-CH_3$ Stretching (cm^{-1})
CA	1032	1735		
DES-MIP			-3371	2956
HDES-MIP	1035	1732	3371	

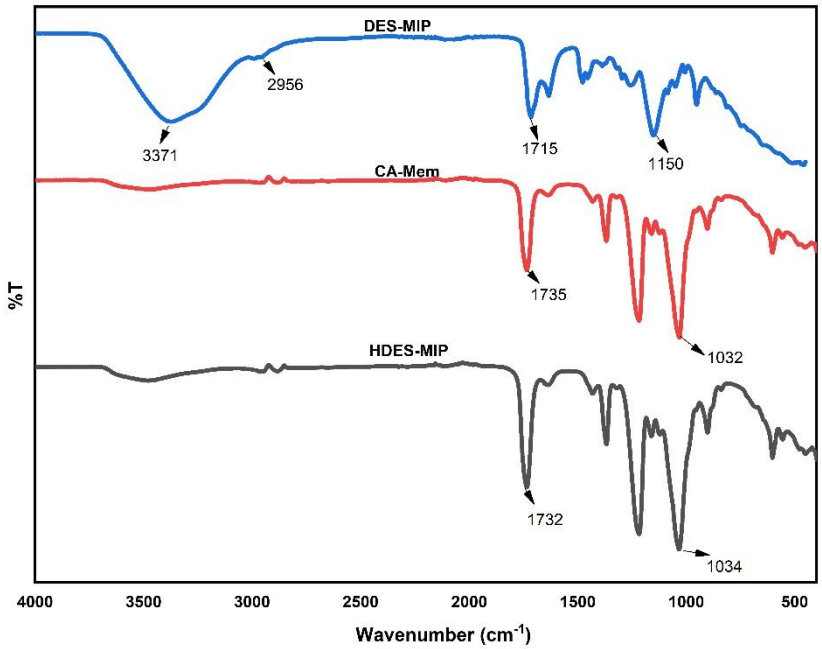

Figure 2. FTIR spectra of DES-MIP particles and HDES-MIP and CA membranes.

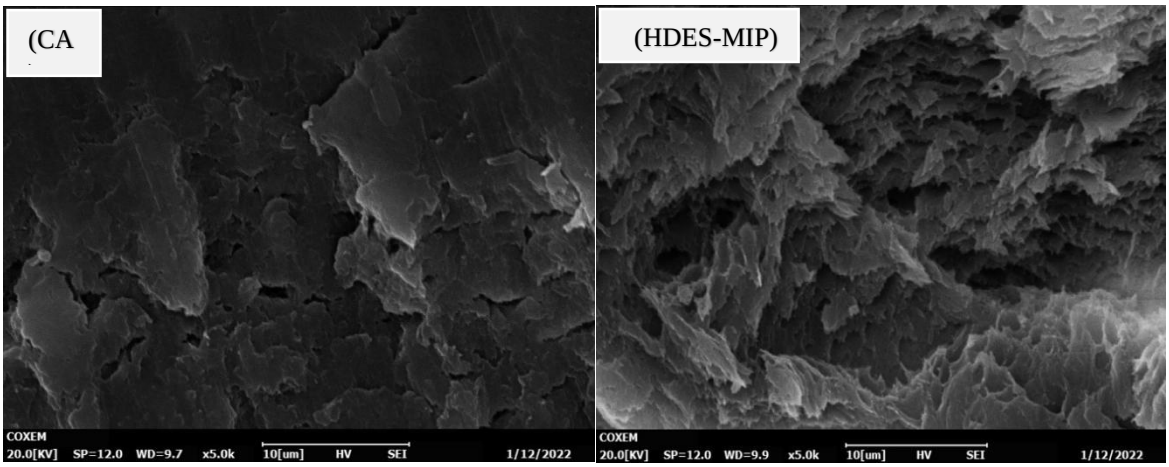

Figure 3. SEM images of the cross-section of (a) CA and (b) HDES-MIP membranes at 5000X magnification.

3. Study of pH Effect

The adsorption of BPA onto the HDES-MIP and CA membranes is shown in Figure 4. The adsorption capacity of the HDES-MIP membrane increased progressively as the pH of the BPA solution increased, reaching a maximum at pH 8. This is because hydrogen bonds and ionic interactions are the main binding forces between BPA and the HDES-MIP membranes. The concentrations of H^+ and OH^- were minimal only in the nearly neutral solution, which reduced their impact and binding force between the sites. The target molecule and BPA binding capability of the CA membrane were lower than those of the HDES-MIP membrane. The adsorption capacity of the CA membrane did not follow any predictable pattern, because it lacked reactive sites. The increased solubility of BPA on the HDES-MIP membrane compared with that on the CA membrane may be the result of stronger interactions between the two compounds. These interactions include dipole-dipole interactions between the HDES-MIP membrane and the adsorbate, as well as van der Waals forces.

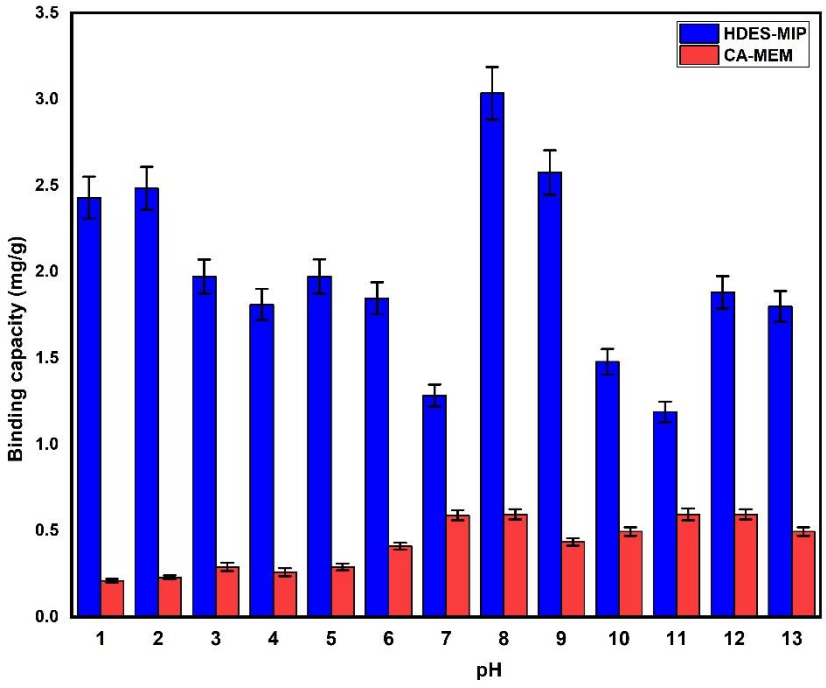

Figure 4. Effect of pH on the binding capacity of BPA to HDES-MIP and CA membranes.

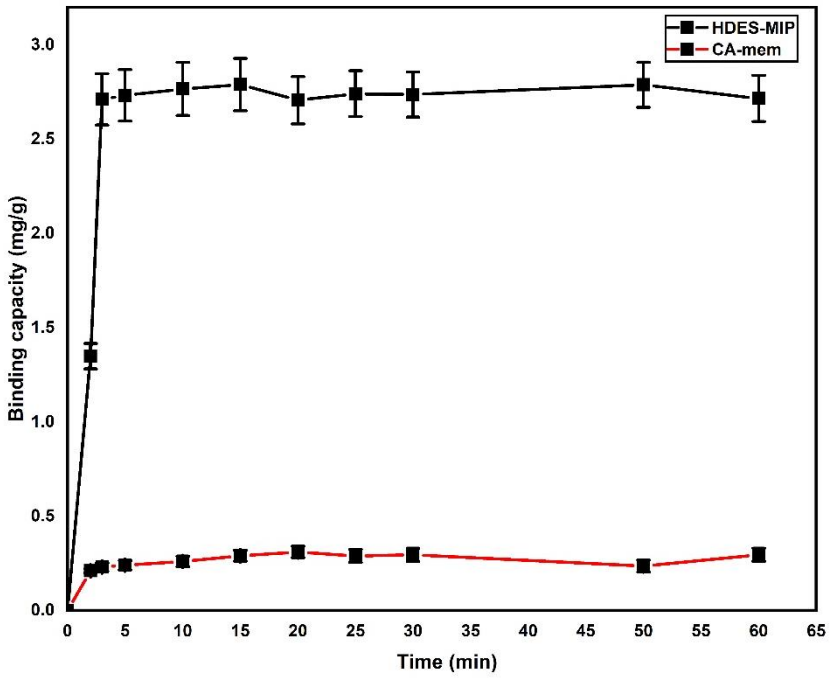

Figure 5. Adsorption kinetics of HDES-MIP and CA membranes.

4. Kinetic Study

It is important to consider sorption kinetics when evaluating the calibration of the sorbent and the effectiveness of the removal process. The reaction was performed at pH 8. The binding capacities of the HDES-MIP and CA membranes were calculated as a function of time. The results are shown in Figure 5. The HDES-MIP membrane grew rapidly during the first 10 min, before settling to equilibrium. This is because, at the start of the reaction, there were more sites on the HDES-MIP membrane's surface. It was easier for equilibrium to develop over time, as more locations were occupied. The CA membrane, on the other hand, did not exhibit a clear pattern of BPA absorption. The CA membrane exhibited very low adsorption capacity owing to the absence of specific cavities. It is evident that the dynamic adsorptive separation of a solute from a solution onto adsorbents requires an accurate depiction of the equilibrium separation between the two phases. The general understanding is that the highest level of absorption occurs when there is a fully saturated monolayer of sorbents on the adsorbent surface and the energy of absorption remains constant without any surface migration [26], [34].

4.1. Pseudo-first-order Kinetic Model

The rate constants of the HDES-MIP and CA membranes are listed in Table 2. The k_1 and R^2 values of the HDES-MIP membrane based on the pseudo-first-order model were determined to be 0.0012 min^{-1} and 0.2494, respectively, as shown in Figure 6. The k_1 and R^2 values of the CA membrane were calculated as 0.0006 min^{-1} and 0.7265, respectively. The q_e values of the HDES-MIP and CA membranes were calculated as 2.873 and 0.6891 mg/g, respectively. The calculated R^2 values of the HDES-MIP and CA membranes were 0.2494 and 0.7265 mg/g, respectively. Based on the experimental and calculated values and the R^2 values, it was concluded that the HDES-MIP and CA membranes did not fit the pseudo-first-order kinetic model.

4.2. Pseudo-second-order Model

The k_2 and R^2 values of the pseudo-second-order model of the HDES-MIP membrane were calculated as 0.8344 min^{-1} and 0.9986, respectively. The k_2 and R^2 values of the CA membrane were calculated as 0.6816 min^{-1} and 0.9936, respectively. The calculated q_e values (q_e cal) of the HDES-MIP and CA membranes were 2.7679 and 0.7013 mg/g, respectively, which are very close to the experimental q_e values (q_e exp) of 2.7821 and 0.6891 mg/g, respectively (Table 2). The pseudo-second-order model and kinetic studies of the HDES-MIP membrane were in good agreement. The chemisorption of BPA on the HDES-MIP membrane was described by a pseudo-second-order model that can be applied to the full sorption process. The rate-limiting phase of chemical sorption may be due to the valence forces resulting from the sharing or exchange of electrons between the sorbent and the sorbate. A similar report had been published previously [35].

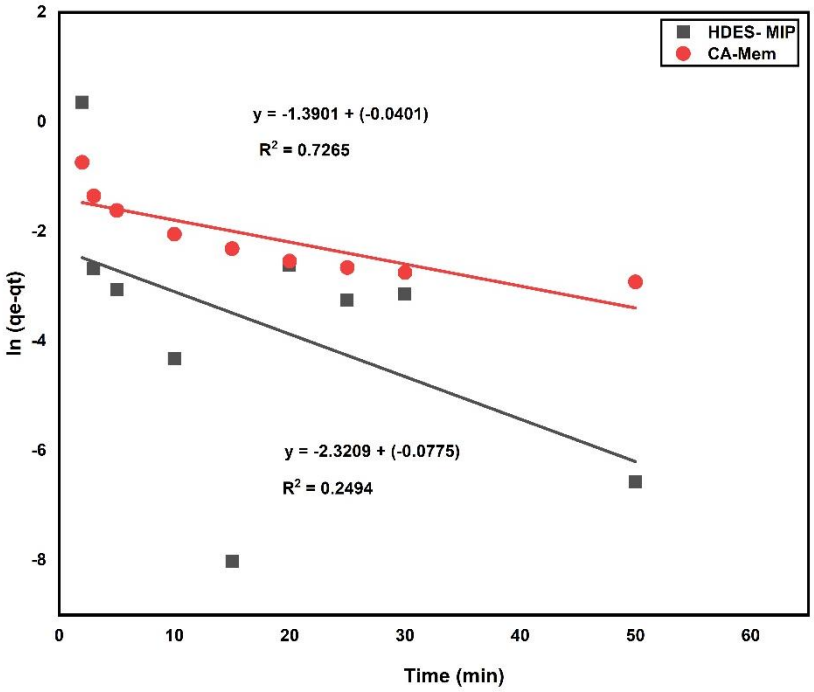

Figure 6. Pseudo-first-order model of HDES-MIP and CA membranes.

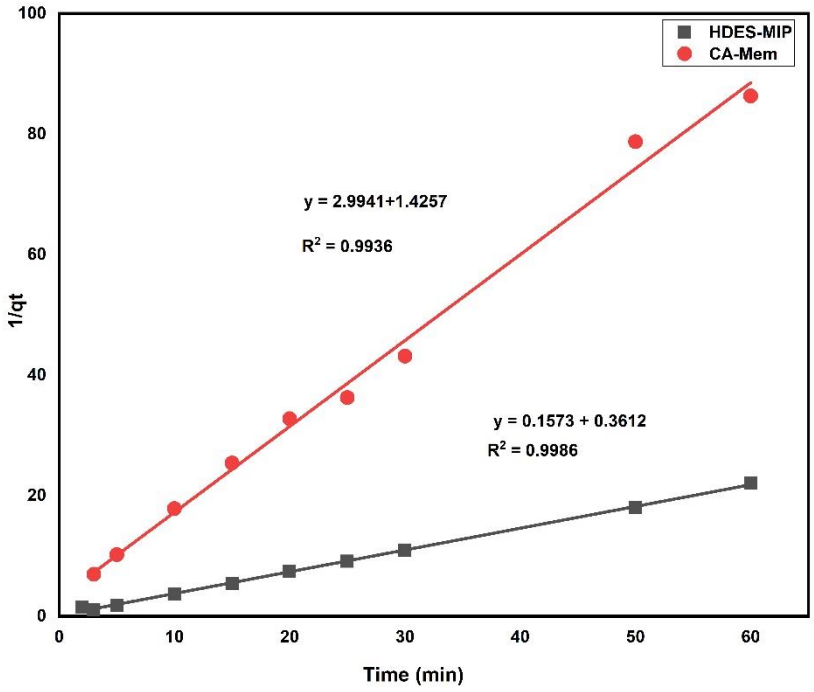

Figure 7. Pseudo-second-order model of HDES-MIP and CA membranes.

Table 2. Kinetic parameters for the sorption of BPA by HDES-MIP and CA membranes.

	Pseudo-first-order kinetic				Pseudo-second-order kinetic		
Membranes	q_e exp (mg/g)	R^2	q_e cal (mg/g)	k_1	R^2	q_e cal (mg/g)	k_2
HDES-MIP	2.7821	0.2494	0.0981	0.0012	0.9986	2.7679	0.8344
CA	0.6891	0.7265	0.2491	0.0006	0.9936	0.7013	0.6816

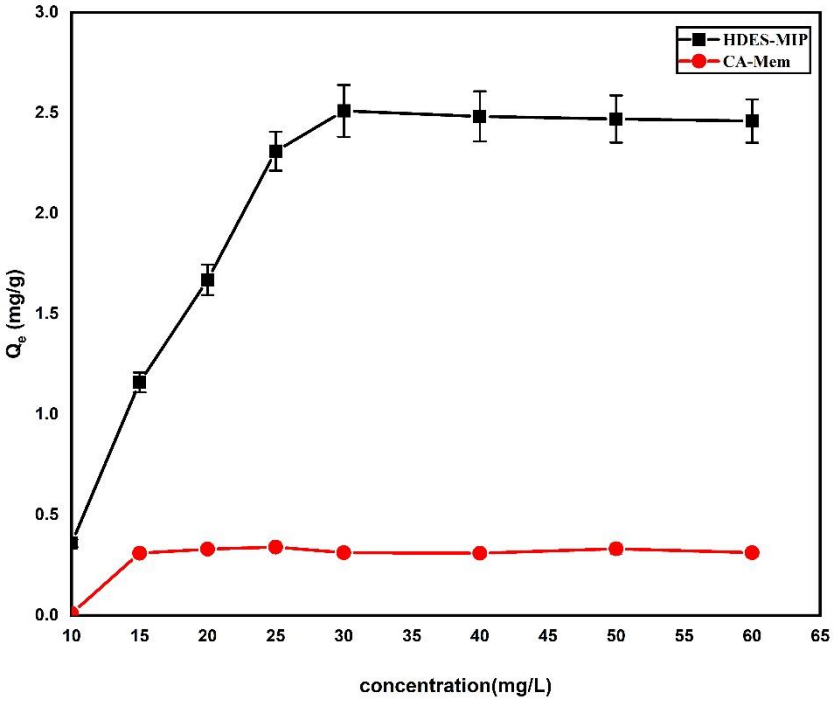

Figure 8. Effect of concentration on the adsorption capacity of HDES-MIP and CA membranes.

5. Isotherm Study

BPA was absorbed at various doses (10, 15, 20, 25, 30, 35, 40, 45, 50, and 60 mg/L) onto the HDES-MIP and CA membranes. With increasing BPA concentration, the adsorption value of the HDES-MIP membrane steadily increased until equilibrium was reached, as shown in Figure 8. The HDES-MIP and CA membranes reached the highest adsorption capacities of 2.56 and 0.41 mg/g, respectively. This is because the HDES-MIP membrane had BPA-imprinted cavities. In contrast, the CA membrane exhibited no distinct change in adsorption as the concentration was changed. It can be said that the HDES-MIP membrane effectively absorbed BPA compared to the CA membrane. Various isothermal models, such as the Freundlich and Langmuir models, were used to identify the adsorption behavior of BPA on both membranes.

5.1. Langmuir Isotherm Model

The sorption mechanism of the HDES-MIP membrane is explained using the Langmuir isotherm model. Higher R^2 values of 0.9188 for the HDES-MIP membrane and 0.7425 for the CA membrane were obtained in the Langmuir plots (Figure 9) (Table 3). The superior R^2 value of the HDES-MIP membrane demonstrates that the Langmuir isotherm model predicts adsorption. The computed values (q_m cal) of HDES-MIP and CA were 2.5610 and 0.4031 mg/g, respectively. These values are close to the experimental data (q_m exp) of the CA (0.2802 mg/g) and HDES-MIP (2.5101 mg/g) membranes. In addition, the dimensionless (R_L) for HDES-MIP and MIP, respectively, was between 0 and 1, supporting the successful implementation of BPA.

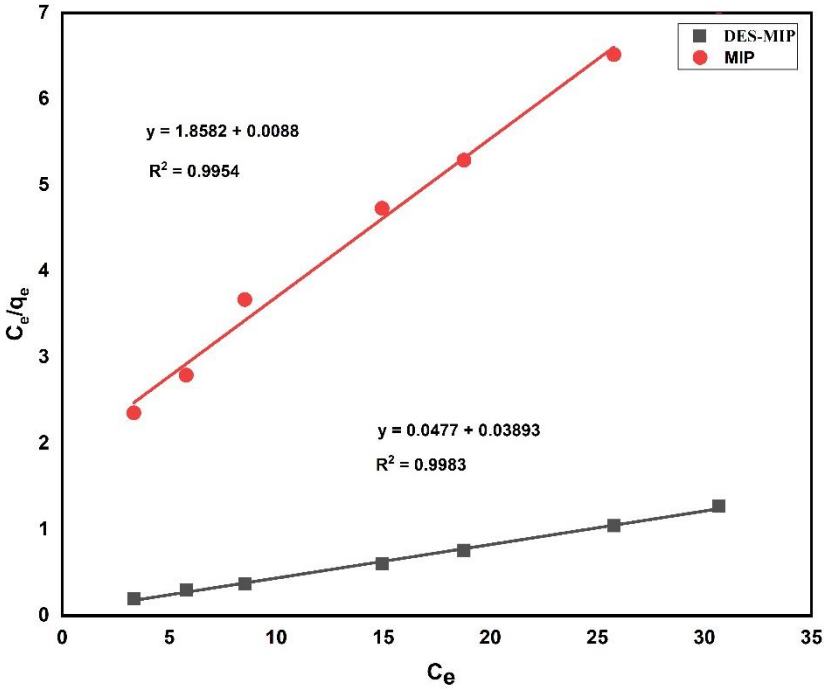

Figure 9. Langmuir isotherm model of HDES-MIP and CA membranes.

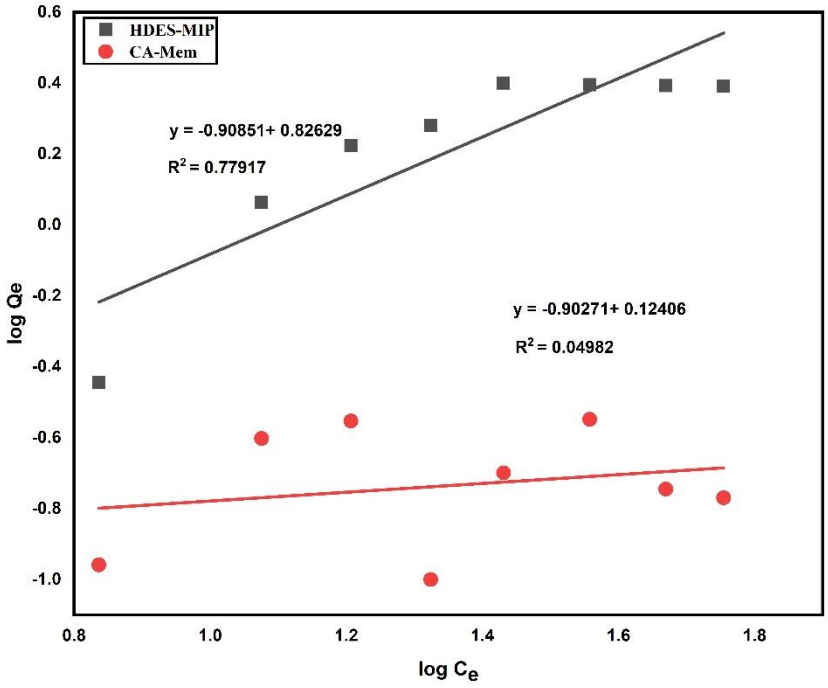

Figure 10. Freundlich isotherm model of HDES-MIP and CA membranes.

Table 3. Isothermal parameters for the sorption of BPA by HDES-MIP and CA membranes.

	Langmuir isotherm model				Freundlich isotherm model		
Membrane	q_m exp (mg/g)	R^2	q_m cal (mg/g)	R_L	R^2	$1/n$	K_f
HDES-MIP	2.5101	0.9188	2.5610	0.2645	0.7791	0.8262	0.1234
CA	0.2802	0.7425	0.4031	0.4307	0.0498	0.1240	0.1251

5.2. Freundlich Isotherm Model

The Freundlich isotherm model assumes that sorption occurs on heterogeneous surfaces and that the absorption capacity is dependent on the equilibrium BPA concentration. The R^2 values for the HDES-MIP and CA membranes were 0.77917 and 0.049982, respectively, as shown in Table 3, and in accordance with the Freundlich isotherm (Figure 10). The K_f values of the HDES-MIP and CA membranes were 0.123 and 0.125, respectively. It was determined that the sorption procedure was unsuitable because of the high K_f value. Therefore, the Langmuir isothermal model was used for the HDES-MIP membranes.

6. Thermodynamic Study

Figure 11 shows the relationship between ln *k* values at three distinct temperatures (298, 318, and 338 K) and the reciprocal of the absolute temperature. With an R^2 value of 0.9856, the HDES-MIP membrane exhibited a straight line at a reciprocal temperature of 1/*T*. The graph demonstrates the relationship between the adsorption of BPA and temperature, as well as the relationship between temperature and adsorption of the HDES-MIP membrane. The slope and linear intercept of ln *k* versus 1/*T* were used to obtain the values of H^o and S^o. Table 4 lists the values of G^o, H^o, and S^o. The results indicated the exothermic nature of BPA adsorption on the HDES-MIP membrane, with the calculated values of ΔH^o and ΔS^o being -39.785 kJ/mol and -151.28 J/Kmol, respectively, indicating that the adsorption of BPA on the HDES-MIP membrane was more effective [28]. The adsorbate molecules and adsorbent surface interacted strongly as a result of the H^0 of the HDES-MIP membrane having a greater value. A spontaneous process in the HDES-MIP membrane, which does not require input energy from outside the system, was also indicated by the lower value of G^0 at 298 K. A lower G^0 value indicates a stronger adsorption driving force, which increases adsorption capacity. As temperature increased, absolute G^0 values shifted towards more positive values, indicating that BPA adsorption was less advantageous [37]. The adsorbed BPA was more advantageous and had a stronger adsorptive affinity for the DES-MIP membrane according to the reasoning given above; however, the CA membrane exhibited the same BPA sorption activity. The amount of BPA that adhered to the CA membrane was not significantly affected by the temperature change. As shown in Figure 10, the CA membrane displayed an R^2 value of 0.4810 in a nonlinear graph. In addition to the H^o and S^o values, the G^o values were also calculated. According to the computed values of H^o and S^o, which were -5.7123 kJ/mol and 18.0348 J/Kmol, respectively, BPA was adsorbed onto the CA membrane and was less effective.

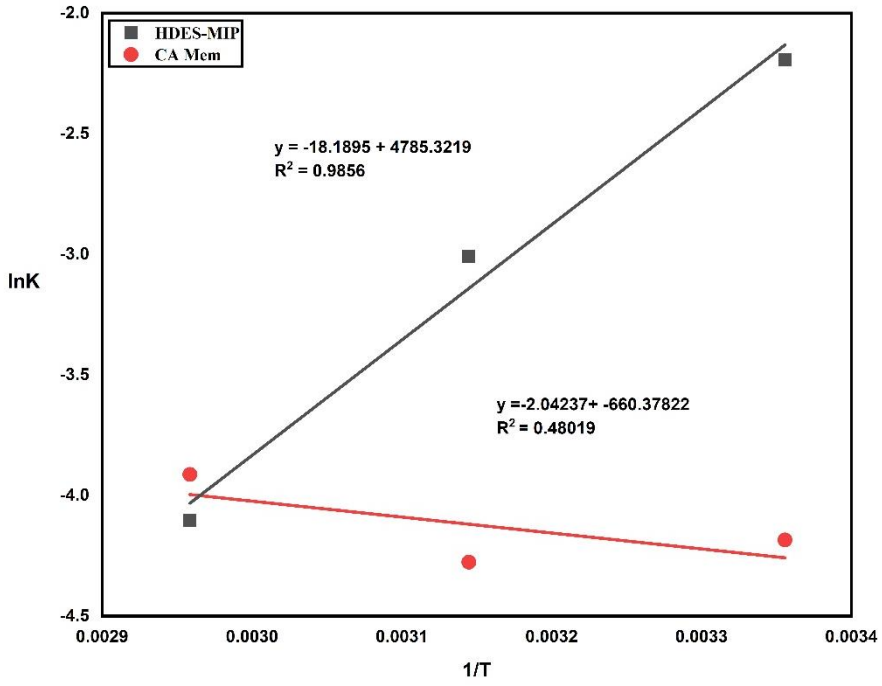

Figure. 11. Thermodynamic effects of HDES-MIP and CA membranes.

Table 4. Thermodynamics of BPA adsorption onto HDES-MIP and CA membranes at different temperatures.

Membranes	Temperature (K)	Enthalpy ΔH° (kJ/mol^{-1})	Entropy ΔS° (J/Kmol)	Gibbs energy ΔG° (kJ/mol^{-1})	R^2
HDES-MIP	298	-39.785	-115.228	5.434	0.9856
	318			7.954	
	338			11.527	
CA	298	-5.7123	18.0348	10.367	0.4801
	318			11.306	
	338			10.994	

CONCLUSION

DES-MIP particles were successfully synthesized via bulk polymerization using BPA as the template, and successfully hybridized with CA to obtain a HDES-MIP membrane. Changes in the fundamental groups and differences in morphology were confirmed by FTIR and SEM. The HDES-MIP membrane showed maximum binding capacity at pH 8. The adsorption kinetic and isothermal studies were in good agreement with the pseudo-first-order kinetic and Langmuir isotherm models, respectively. Thermodynamic studies indicated that the adsorption of BPA on the HDES-MIP membrane was exothermic. The negative enthalpy values in thermodynamics also indicate that the HDES-MIP membrane underwent exothermic and spontaneous reactions. These findings suggest that HDES-MIP has excellent potential for BPA removal. Thermodynamic analyses indicated that the adsorption process was exothermic and spontaneous. These findings highlight the potential of HDES-MIP as an effective and environment-friendly solution for the removal of BPA contaminants, which is important for addressing pollution concerns and advancing sustainable materials. This study contributes to the field of environmental remediation and offers a promising approach for mitigating BPA pollution.

ACKNOWLEDGMENT

This research was supported by the Ministry of Higher Education (MOHE) through the Fundamental Research Grant Scheme for Research Acculturation of Early Career Research (FRGS-Racer) RACER/1/2019/STG01/UTHM//2 and Research Grant Scheme (FRGS)/1/2022/TK05/UTHM/03/10 and assistance from Universiti Tun Hussein Onn Malaysia (UTHM).

REFERENCES

1. Bertanza, G., *et al.* (2011) Effect of biological and chemical oxidation on the removal of estrogenic compounds (NP and BPA) from waste-water: An integrated assessment procedure. *Water Res*, **45**, 8, 2473–2484. doi: 10.1016/j.watres.2011.01.026.

2. Gallo, P., *et al.* (2017) Determination of BPA, BPB, BPF, BADGE and BFDGE in canned energy drinks by molecularly imprinted polymer cleaning up and UPLC with fluorescence detection. *Food Chem*, **220**, 406–412.

3. Zhang, N., Scarsella, J. B. and Hartman, T. G. (2020) Identification and quantitation studies of migrants from bpa alternative food-contact metal can coatings. *Polymers (Basel)*, **12**, 2, 1–13.

4. Guo, W., *et al.* (2011) Selective adsorption and separation of BPA from aqueous solution using novel molecularly imprinted polymers based on kaolinite/Fe3O4 composites. *Chemical Engineering Journal*, **171**, 2, 603–611.

5. Wassenaar, P. N. H., Rorije, E., Vijver, M. G. and Peijnenburg, W. J. G. M. (2021) Evaluating chemical similarity as a measure to identify potential substances of very high concern. *Regulatory Toxicology and Pharmacology*, **119**, 104834, October 2020.

6. Yu, L., Wang, C., Ren, X. and Sun, H. (2014) Catalytic oxidative degradation of bisphenol A using an ultrasonic-assisted tourmaline-based system: Influence factors and mechanism study. *Chemical Engineering Journal*, **252**, 346–354. 10.1016/j.cej.2014.05.014.

7. Yamanaka, H., Moriyoshi, K., Ohmoto, T., Ohe, T. and Sakai, K. (2008) Efficient Microbial Degradation of Bisphenol A in the Presence of Activated Carbon. *J Biosci Bioeng*, **105**, 2, 157–160. doi: 10.1263/jbb.105.157.

8. Marfà, J., Pupin, R. R., Sotomayor, M. and Pividori, M. I. (2021) Magnetic-molecularly imprinted

polymers in electrochemical sensors and biosensors. *Anal Bioanal Chem*, **413**, 24, 6141–6157.

9. Yang, G., Liu, H., Wang, M., Liu, S. and Chen, Y. (2006) Chromatographic characterization and solid-phase extraction on diniconazole-imprinted polymers stationary phase. *React Funct Polym*, **66**, 5, 579–583.

10. Walshe, M., Garcia, E., Howarth, J., Smyth, M. R. and Kelly, M. T. (1997) Separation of the Enantiomers of Propranolol by Incorporation of Molecularly Imprinted Polymer Particles as Chiral Selectors in Capillary Electrophoresis. *Analytical Communications*, **34**, 4, 119–122. doi: 10.1039/a701250k.

11. Liu, J., *et al.* (2011) A novel polychloromethylstyrene coated superparamagnetic surface molecularly imprinted core-shell nanoparticle for bisphenol A. *J Mater Chem*, **21**, 25, 9232–9238. doi: 10.1039/c1jm10227c.

12. Chen, B., Jiang, C., Yu, D., Wang, Y. and Xu, T. (2020) Design of an alternative approach for synergistic removal of multiple contaminants: Water splitting coagulation. *Chemical Engineering Journal*, **380**, 122531, August 2019. doi: 10.1016/j.cej.2019.122531.

13. Saleh, I. A., Zouari, N. and Al-Ghouti, M. A. (2020) Removal of pesticides from water and wastewater: Chemical, physical and biological treatment approaches. *Environ Technol Innov*, **19**, 101026.

14. Yang, Z., Zhang, Y., Zhu, W., Zan, X., Zhang, L. and Liu, Y. (2020) Effective oxidative degradation of coal gasification wastewater by ozonation: A process study. *Chemosphere*, **255**, 126963.

15. Liu, Q., *et al.* (2021) Activated carbon prepared from catechol distillation residue for efficient adsorption of aromatic organic compounds from aqueous solution. *Chemosphere*, **269**, 128750.

16. Arabi, M., *et al.* (2020) Strategies of molecular imprinting-based solid-phase extraction prior to chromatographic analysis. *TrAC - Trends in Analytical Chemistry*, **128**, 115923.

17. Jablonský, M., Majová, V., Šima, J., Hroboňová, K. and Lomenová, A. (2020) Involvement of deep eutectic solvents in extraction by molecularly imprinted polymers—a minireview. *Crystals (Basel)*, **10**, 3, 1–12.

18. Xu, K., Wang, Y., Wei, X., Chen, J., Xu, P. and Zhou, Y. (2018) Preparation of magnetic molecularly imprinted polymers based on a deep eutectic solvent as the functional monomer for specific recognition of lysozyme. *Microchimica Acta*, **185**, 2.

19. Fu, N., *et al.* (2017) Specific recognition of polyphenols by molecularly imprinted polymers based on a ternary deep eutectic solvent. *J Chromatogr A.*, **1530**, 23–34.

20. Piletsky, S. A., Panasyuk, T. L., Piletskaya, E. V., Nicholls, I. A. and Ulbricht, M. (1999) Receptor and transport properties of imprinted polymer membranes - A review. *J Memb Sci*, **157**, 2, 263–278. doi: 10.1016/S0376-7388(99)00007-1.

21. Ciardelli, G., Borrelli, C., Silvestri, D., Cristallini, C., Barbani, N. and Giusti, P. (2006) Supported imprinted nanospheres for the selective recognition of cholesterol. *Biosens Bioelectron*, **21**, 12, 2329–2338.

22. Trotta, F., Baggiani, C., Luda, M. P., Drioli, E. and Massari, T. (2005) A molecular imprinted membrane for molecular discrimination of tetracycline hydrochloride. *J Memb Sci*, **254**, 1–2, 13–19.

23. Pan, Z., *et al.* (2022) A recognition strategy combining effective boron affinity technology and surface imprinting to prepare highly selective and easily recyclable polymer membrane for separation of drug molecule. *J Colloid Interface Sci*, **624**, 1–13, Oct. 2022. doi: 10.1016/j.jcis.2022.05.138.

24. Piloto, A. M. L., Ribeiro, D. S. M., Rodrigues, S. S. M., Santos, J. L. M., Sampaio, P. and Sales, G. (2021) Imprinted Fluorescent Cellulose Membranes for the On-Site Detection of Myoglobin in Biological Media. *ACS Appl Bio Mater*, **4**, 5, 4224–4235, May 2021. doi: 10.1021/acsabm.1c00039.

25. Algieri, C., Drioli, E., Guzzo, L. and Donato, L. (2014) Bio-mimetic sensors based on molecularly imprinted membranes. *Sensors*, **14**, 8, 13863–13912.

26. Shah, S. A. H. and Asman, S. (2023) Evaluation of deep eutectic solvent as a new monomer for molecularly imprinted polymers for removal of bisphenol A. *Journal of Polymer Research*, **30**, 6, Jun. 2023. doi: 10.1007/s10965-023-03581-1.

27. Yusof, N. A., Zakaria, N. D., Maamor, N. A. M., Abdullah, A. H. and Haron, M. J. (2013) Synthesis and characterization of molecularly imprinted polymer membrane for the removal of 2,4-dinitrophenol. *Int J Mol Sci*, **14**, 2, 3993–4004.

28. Berber, A., Gürdal, M. and Bağırsakçı, K. (2021) Prediction of heat transfer in a circular tube with aluminum and Cr-Ni alloy pins using artificial

neural network. *Experimental Heat Transfer*, **34**, 6, 547–563.

29. Ezzati, R. (2020) Derivation of Pseudo-First-Order, Pseudo-Second-Order and Modified Pseudo-First-Order rate equations from Langmuir and Freundlich isotherms for adsorption. *Chemical Engineering Journal*, **392**, 123705, September 2019.

30. Lu, Y. C., Xiao, W. W., Wang, J. Y. and Xiong, X. H. (2021) Rapid isolation and determination of bisphenol A in complicated matrices by magnetic molecularly imprinted electrochemical sensing. *Anal Bioanal Chem*, **413**, 2, 389–401. doi: 10.1007/s00216-020-03006-8

31. Asman, S., Mohamad, S. and Sarih, N. M. (2016) Study of the morphology and the adsorption behavior of molecularly imprinted polymers prepared by reversible addition-fragmentation chain transfer (RAFT) polymerization process based on two functionalized β-cyclodextrin as monomers. *J Mol Liq*, **214**, 59–69.

32. Abbas, M. (2020) Modeling of adsorption isotherms of heavy metals onto Apricot stone activated carbon: Two-parameter models and equations allowing determination of thermodynamic parameters. *Mater Today Proc*, **43**, 3359–3364.

33. Rojas, G., Silva, J., Flores, J. A., Rodriguez, A., Ly, M. and Maldonado, H. (2005) Adsorption of chromium onto cross-linked chitosan. *Sep Purif Technol*, **44**, 1, 31–36.

34. Yusof, N. A., Rahman, S. K. A., Hussein, M. Z. and Ibrahim, N. A. (2013) Preparation and characterization of molecularly imprinted polymer as SPE sorbent for melamine isolation. *Polymers (Basel)*, **5**, 4, 1215–1228.

35. Zhang, C., Zhong, S. and Yang, Z. (2008) Cellulose acetate-based molecularly imprinted polymeric membrane for separation of vanillin and o-vanillin. *Brazilian Journal of Chemical Engineering*, **25**, 2, 365–373.

36. Mohamed Idris, Z., Hameed, B. H., Ye, L., Hajizadeh, S., Mattiasson, B. and Mohd Din, A. T. (2020) Amino-functionalised silica-grafted molecularly imprinted polymers for chloramphenicol adsorption. *J Environ Chem Eng*, **8**, 5.

37. Mobasherpour, I., Salahi, E. and Ebrahimi, M. (2014) Thermodynamics and kinetics of adsorption of Cu(II) from aqueous solutions onto multi-walled carbon nanotubes. *Journal of Saudi Chemical Society*, **18**, 6, 792–801.